Electrochimica Acta 54 (2008) 566–573

Contents lists available at ScienceDirect

Electrochimica Acta

journal homepage: www.elsevier.com/locate/electacta

Oxygen reduction behavior of rutile-type iridium oxide in sulfuric acid solution

Norihiro Yoshinaga, Wataru Sugimoto, Yoshio Takasu*

Department of Fine Materials Engineering, Faculty of Textile Science and Technology, Shinshu University, 3-15-1 Tokida, Ueda 386-8567, Japan

ARTICLE INFO

Article history:
Received 21 December 2007
Received in revised form 11 July 2008
Accepted 13 July 2008
Available online 22 July 2008

Keywords:
Iridium oxide
Oxygen reduction reaction
Electrocatalyst
Fuel cell
Oxide cathode

ABSTRACT

Two different forms of rutile-type iridium oxide catalysts were prepared: IrO_2-coated titanium plate electrocatalysts prepared by a dip-coating method (IrO_2/Ti) and iridium oxide nanoparticles (IrO_2) prepared by a wet method, the Adams fusion method. The catalytic behavior of the oxygen reduction reaction (ORR) was evaluated by cyclic voltammetry in 0.5 M H_2SO_4 at 60 °C. Both catalysts were found to exhibit considerable activity for the ORR; however, the former oxide electrodes showed higher activity than the latter ones. All the IrO_2/Ti catalyst electrodes heat-treated at a temperature between 400 °C and 550 °C showed ca. 0.84 V (vs. RHE) of the onset potential for the ORR, E_{ORR}, where the reduction current of oxygen had begun to be observed during the cathodic potential sweep of the test electrodes. It has been confirmed clearly that IrO_2, but neither metallic Ir nor the hydrated IrO_2, behaves as an active catalyst for the ORR in an acidic solution. It was also demonstrated that the enlargement of the surface area of the IrO_2/Ti with the help of lanthanum is effective for the enhancement of the catalytic activity in the reaction.

1. Introduction

Fuel cells have attracted the public's attention from both an environmental and a convenience perspective but the technology has not yet become beneficial to the public in terms of availability, cost, durability, size, and so forth.

Although the typical cathode catalyst used for polymer electrolyte fuel cells (PEFCs) is PtCo/C, due to its high oxygen reduction activity [1–4], further enhancement of both catalytic activity and durability is needed before its use becomes practical. The overpotential for the oxygen reduction reaction (ORR) needs to be reduced, and the dissolution of the metal elements has to be minimized [5]. Various approaches have been conducted to overcome these problems, including alloying Pt with other metals and searching for other suitable compounds, including oxides [6–8], carbides [9,10], nitrides, silicides, metal complexes [11,12], and other compounds [13–16]. Recently, some interesting studies on the development of Pt-free oxide cathodes, such as $TaO_{0.92}N_{1.05}$ and ZrO_{2-x}, have been reported [17,18]. Although these and numerous other studies have significantly contributed to the development of PEFC and DMFC, further investigation is still required for the improvement of both activity and durability. Iridium oxide is a typical material that resists corrosion in acidic solutions. Since IrO_2 is one of the outstanding electrocatalysts for oxygen evolution, IrO_2–Ta_2O_5/Ti electrodes [19,20] have been used as oxygen-evolving anodes in the industrial electro-plating process. The IrO_2–RuO_2–TiO_2/Ti ternary oxide electrode is widely used as the Dimensionally Stable Anode (DSA®) catalyst electrode in the electrolysis process for chlorine production in chlor-alkali industries [21]. Although basic investigations on the ORRs of iridium metal [22,23], iridium alloy electrodes [24,25], unhydrated or hydrated iridium oxide as support of platinum particles [26,27] as well as the ORR of iridium oxide in an alkaline solution [28,29] have been published. Studies on crystalline iridium oxide in acidic solutions have scarcely been reported on to date [30,31]. In previous investigations [30,31], these authors reported results concerning the ORR activity of a dip-coated IrO_2/Ti electrocatalyst.

This study presents fundamental results on the iridium oxide catalysts for ORR, using both iridium oxide coated on a Ti plate substrate prepared by a dip-coating method (IrO_2/Ti) and IrO_2 nanoparticles prepared by a wet method, the Adams fusion method. Besides the fundamental information on the electrocatalytic property of IrO_2, the results must provide ideas to design less-expensive oxide cathode catalysts for the ORR.

2. Experimental

2.1. Preparation of IrO_2/Ti electrodes by a dip-coating method

Rutile-type IrO_2-coating film was prepared on a Ti plate (10 mm × 10 mm × 1 mm) substrate by a conventional dip-coating method using a butanolic solution of iridium chloride ([$IrCl_3$] = 0.5 M). The titanium substrates were etched with 10% oxalic acid at 80 °C for 1 h, and then rinsed with deionized water

* Corresponding author. Tel.: +81 268 21 5451; fax: +81 268 22 9048.
E-mail address: ytakasu@shinshu-u.ac.jp (Y. Takasu).

0013-4686/$ – see front matter © 2008 Elsevier Ltd. All rights reserved.
doi:10.1016/j.electacta.2008.07.020

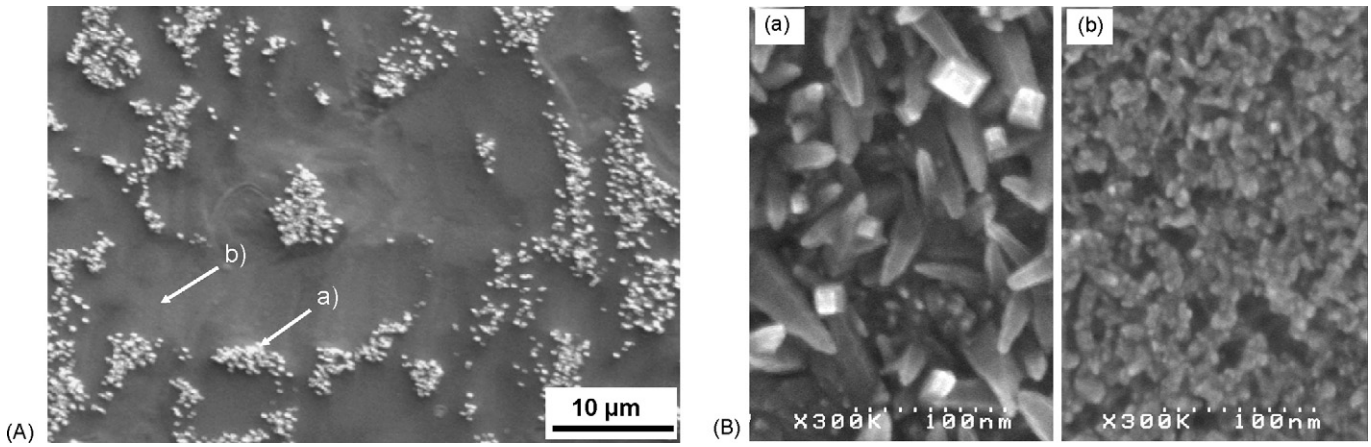

Fig. 1. (A) A typical SEM image of an IrO_2/Ti electrode prepared by the dip-coating method at 450 °C: the crystallites part (a) and the flat part (b). (B) High magnification SEM images of the crystallites part (a) and the flat part (b) shown in Fig. 1(A).

before the dipping procedure. Calcination of the dip-coated salts was conducted at various air temperatures between 400 °C and 550 °C. The dip-drying/calcination (alternating 10 min each) procedure was repeated seven times. An IrO_2/Ti electrode with extremely enlarged surface area was prepared using a dip-coating solution containing $IrCl_3$ and $LaCl_3$ in butanol ($[IrCl_3] = [LaCl_3] = 0.5$ M) [32,33]. After the dip-drying/calcination (450 °C, 10 min) procedure was repeated seven times, any of the lanthanum species were completely removed with 0.5 M H_2SO_4 at 60 °C. No traces of lanthanum species were detected after the acid treatment. This electrode was denoted to be La_2O_3-treated IrO_2/Ti electrode in this study.

2.2. Preparation of IrO_2 nanoparticles by the Adams fusion method

Iridium oxide powder, IrO_2, was prepared by the Adams fusion method [34]. A metal precursor ($H_2IrCl_6{\cdot}nH_2O$) was added to 10 mL of 2-propanol to achieve a total metal concentration of 0.07 mol L^{-1}. This was magnetically stirred for 2 h to ensure complete dissolution of the precursor; this was followed by the addition of 10 g of finely ground $NaNO_3$. This solution–$NaNO_3$ mixture was heated at an air temperature of 70 °C until completely dry. The dry salt mixture was then placed into a preheated furnace between 400 °C and 500 °C for 30 min. The fused salt–oxide mixture was cooled down slowly to room temperature, then washed three times in deionized water to remove the remaining salts. The iridium oxide was separated by centrifugation and the recovered oxide powder dried in air at 70 °C.

2.3. Electrochemical measurements

The ORR activity of these oxide electrodes was evaluated by cyclic voltammetry (CV) in 0.5 M H_2SO_4 using a beaker-type electrolytic cell, in a stationary state at 60 °C. The test electrode of the IrO_2 nanoparticles was prepared using the thin-film electrode method [35,36]. Briefly, 10 μg of the oxide powder was dispersed in 10 mL of water and was subjected to ultrasonification for 30 min. Then, 40 μL of the oxide powder dispersion was dropped onto a mirror-polished glassy carbon (GC) of the rotating disk electrode (0.196 cm^2 exposed surface). After drying at 60 °C, 20 μL of a 0.03 wt.% Nafion® alcoholic dispersion was also dropped onto the electrode surface to stabilize the oxide particles on the GC surface.

A carbon felt, rather than Pt, was used as the counter electrode in order to avoid the deposition of Pt onto the test electrode through dissolution. Although an Ag/AgCl reference electrode was used, the electrode potential is presented vs. RHE. A Luggin capillary faced the working electrode at a distance of 2 mm. All electrode potentials are referred to the RHE(t) scale, corrected for temperature effect. For the ORR experiment, oxygen gas was bubbled into the 0.5 M H_2SO_4 solution at 60 °C.

3. Results and discussion

3.1. Surface morphology and structure of IrO_2/Ti electrodes prepared at various temperatures

The IrO_2/Ti electrodes prepared by this dip-coating method show typical surface morphology and crystal structure, as reported in many studies so far [37–41]. The typical scanning electron micrograph (SEM) of an IrO_2/Ti electrode prepared at 450 °C is shown in Fig. 1(A) and (B). The white particles seen in the SEM image are IrO_2 crystallites (Fig. 1(B)-(a)), and the flat part is also composed of fine IrO_2 particles that are connected to each other to form a porous structure (Fig. 1(B)-(b)). The X-ray diffraction (XRD) patterns of the IrO_2/Ti electrodes prepared at various temperatures between 400 °C and 550 °C are shown in Fig. 2. These patterns show that

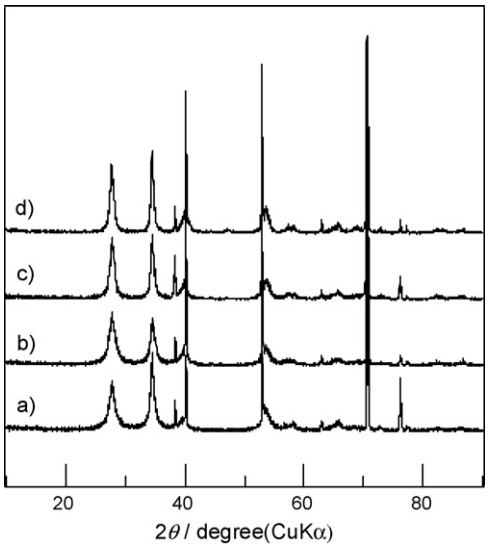

Fig. 2. XRD patterns of IrO_2/Ti electrodes prepared at various temperatures by the dip-coating method. Preparation temperatures: (a) 400 °C, (b) 450 °C, (c) 500 °C, and (d) 550 °C.

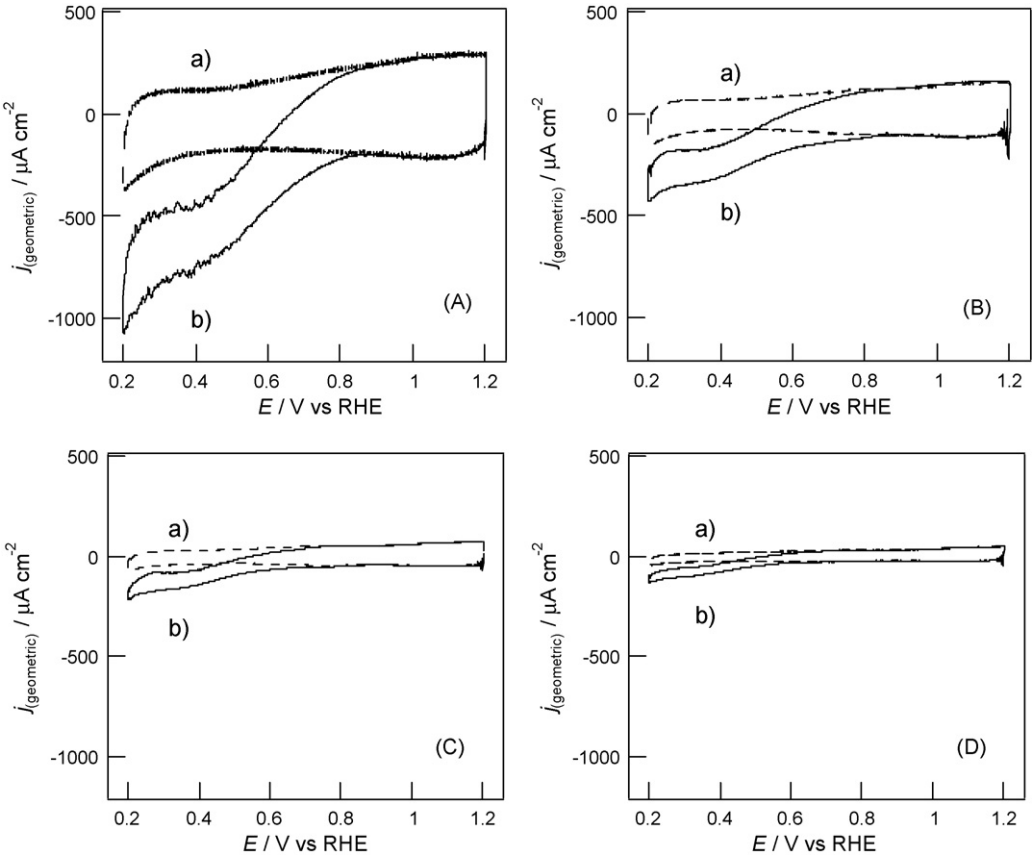

Fig. 3. Cyclic voltammograms of IrO_2/Ti electrodes prepared at various temperatures. Preparation temperatures: (A) 400 °C, (B) 450 °C, (C) 500 °C, and (D) 550 °C. Electrolytes: broken lines (a), in N_2-saturated 0.5 M H_2SO_4, 60 °C; solid lines (b), in O_2-saturated 0.5 M H_2SO_4, 60 °C. Electrode potential sweep rate: 5 mV s^{-1}.

rutile-type IrO_2 was formed on the Ti substrate under the preparation temperatures. Both the intensity and half-width of these diffraction peaks, especially the (1 1 0) diffraction peak at $2\theta = 27.7°$, show that the crystallinity of IrO_2 increases with heat-treatment temperature.

3.2. ORR behavior of IrO_2/Ti electrodes

Fig. 3 shows CVs of the IrO_2/Ti electrodes heat-treated at various temperatures for 10 min, between 400 °C and 550 °C, in N_2-saturated 0.5 M H_2SO_4 (dotted lines (a)) and in O_2-saturated 0.5 M H_2SO_4 (solid lines (b)). During both potential scans (anodic and cathodic potential sweeps), an additional cathodic current was observed for those CVs measured with an O_2-saturated solution, as compared with those measured with an N_2-saturated solution. This additional cathodic current is due to the ORR on each of the oxide electrodes. Fig. 4 shows the ORR cathodic current curves presented in each geometric surface area, for the electrodes, which were obtained by subtracting the voltammogram of the O_2-saturated solution during a cathodic scan from that of the N_2-saturated electrolytes. With an increase in heat-treatment temperature, the cathodic current for the ORR decreases. In order to clarify the effect of the heat-treatment temperature of IrO_2/Ti on the current density, the current densities per effective surface area of these electrodes must be compared, where the effective surface area does not mean the real surface area determined by the BET (Burnauer–Emmett–Teller) method but the surface area which contributes to the ORR reaction under static condition without rotating of the test electrode in the electrolyte. Although it is not easy to determine the effective surface area of these electrodes in the ORR reaction, the current densities for the ORR on these electrodes can be estimated by the division of the current shown in Fig. 4 with the pseudo-capacitance of these IrO_2/Ti electrodes. The estimated surface area (ESA) of these electrodes was evaluated using the cyclic voltammograms measured on the N_2-saturated electrolytes shown in Fig. 3, assuming that of the monolayer capacitance of the IrO_2 was 80 μF cm^{-2}, the same as that of RuO_2 [42,43]. The *j*–*E* curves of these electrodes are shown in Fig. 5. Since the voltammetry was carried out under a stationary state, the ORR-

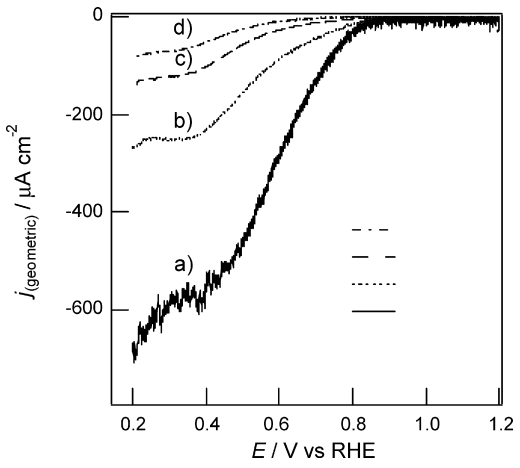

Fig. 4. ORR-current curves of IrO_2/Ti electrodes prepared at various temperatures. Preparation temperatures: (a) 400 °C, (b) 450 °C, (c) 500 °C, and (d) 550 °C. Electrolyte: 0.5 M H_2SO_4, 60 °C. Electrode potential sweep rate: 5 mV s^{-1}.

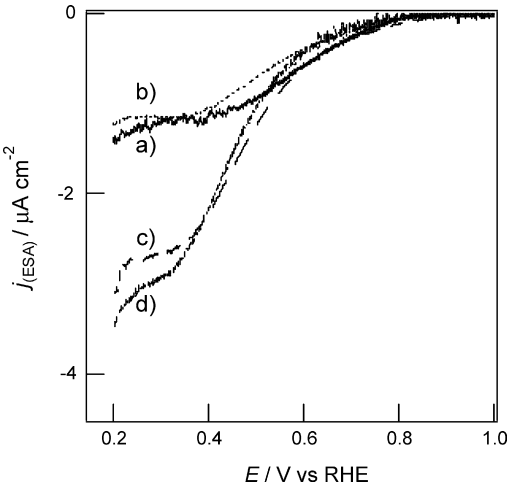

Fig. 5. ORR-current curves presented by current density determined by the estimated surface area (ESA) which was evaluated with the pseudo-capacitance of each IrO_2/Ti electrode prepared at various temperatures. Preparation temperatures: (a) 400 °C, (b) 450 °C, (c) 500 °C, and (d) 550 °C. Electrolyte: 0.5 M H_2SO_4, 60 °C. Electrode potential sweep rate: 5 mV s^{-1}. The estimated surface area (ESA) of these electrodes was evaluated using the cyclic voltammograms measured on the N_2-saturated electrolytes shown in Fig. 3, assuming that of the monolayer capacitance of the IrO_2 was 80 μF cm^{-2}.

current densities of these electrodes must be compared carefully; however, the *j*–*E* curve characteristics of these electrodes with a current density (*j*) lower than ca. 0.5 μA cm^{-2} are almost the same. This strongly suggests that the quality of the active sites of these IrO_2/Ti electrodes for the ORR was the same, even if heat-treatment temperature was different under these conditions. The E_{ORR} values, which mean the electrode potential where the reduction current of oxygen that began to be observed during the cathodic potential sweep of the test oxide electrodes of these electrodes may also be the same, ca. 0.84 V (vs. RHE). The IrO_2 layers of these IrO_2/Ti electrodes were not hydrated oxide but anhydrous oxide, because the XRD peak intensity of these electrodes were strong (Fig. 2) and the profiles of the cyclic voltammograms of them in N_2-saturated solution (Fig. 5) were almost same in spite of the decrease in the pseudo-capacitance with the preparation temperature. However, a more precise examination of the current density and the E_{ORR} is needed to understand the effect of heat-treatment temperature on the quality of the active sites on the IrO_2/Ti catalyst electrode. In particular, the potential effect of titanium ions diffused from the oxide/titanium interface to the IrO_2 oxide layer, when the electrode is heat-treated at high temperature, must be checked. In spite of the potential effect of titanium ions from the oxide/titanium interface, DSA-type electrodes have many advantages: the coating layer is composed of fine oxide particles connected to each other to form a micro/mesoporous structure, the titanium substrate is protected from corrosion by the formation of a dense oxide layer at the interface between the porous oxide coating and titanium substrate, and preparation of the electrodes is easy and useful for the search of new electrocatalysts.

3.3. Enhancement of the ORR activity of IrO_2/Ti electrode

In order to find any methods to enhance the ORR activity of less-expensive oxides, the authors have examined the enhancement of the catalytic activity of IrO_2/Ti electrode for the ORR using two different methods. The first method is the formation of a solid solution to change the valency of iridium ions with another element, vanadium for example [31], and the second one is the use of rare earth elements to enlarge the surface area of oxides [32,33]. When

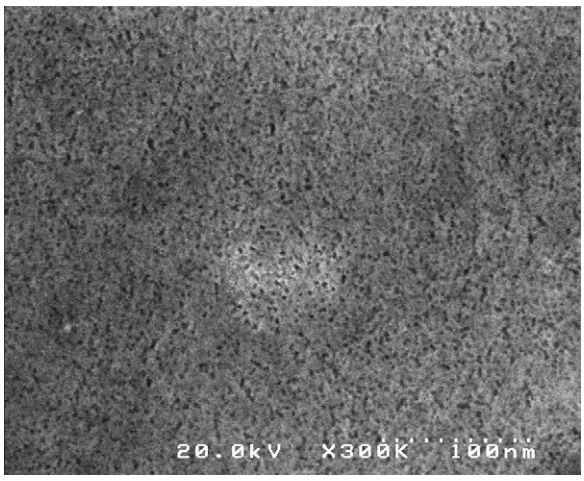

Fig. 6. A typical SEM image of a La_2O_3-treated IrO_2/Ti electrode.

a DSA-type binary oxide electrode was prepared with a dip-coating solution containing iridium salt and a rare earth salt, the resulting electrode was composed of a composite oxide of each element so long as the calcination temperature was not too high. Since the rare earth oxide can easily be removed by acid, a porous IrO_2 layer with extremely enlarged surface area remained after the acid treatment of the composite electrode.

A typical SEM image of a La_2O_3-treated IrO_2/Ti electrode presented in Fig. 6 shows no existence of large crystallites besides many mesopores. An elemental X-ray analysis showed no trace of lanthanum remained in the oxide coating after the acid treatment. A steady-state cyclic voltammogram of this electrode is given in Fig. 7 with that of the IrO_2/Ti electrode prepared at 450 °C already presented in Fig. 3(b) for comparison. The pseudo-capacitance of the former electrode, (a), is about 8.5 times as large as that of the latter one, (b). Therefore, an IrO_2/Ti electrode with highly enlarged surface area was prepared by the dip-coating method with the help of lanthanum during the preparation procedure of the electrode. Fig. 8 shows the ORR behavior of three different oxide electrodes prepared at 450 °C; the IrO_2/Ti electrode, the La_2O_3-treated IrO_2/Ti electrode, and the porous $Ir_{0.6}V_{0.4}O_2$/Ti electrode,

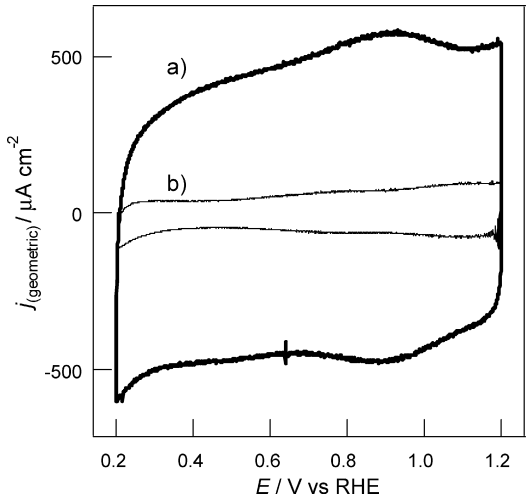

Fig. 7. Steady-state cyclic voltammograms of a La_2O_3-treated IrO_2/Ti electrode and of the IrO_2/Ti electrode prepared at 450 °C presented in Fig. 3(b). Electrodes: (a) La_2O_3-treated IrO_2/Ti electrode and (b) IrO_2/Ti electrode prepared at 450 °C presented in Fig. 3(b).

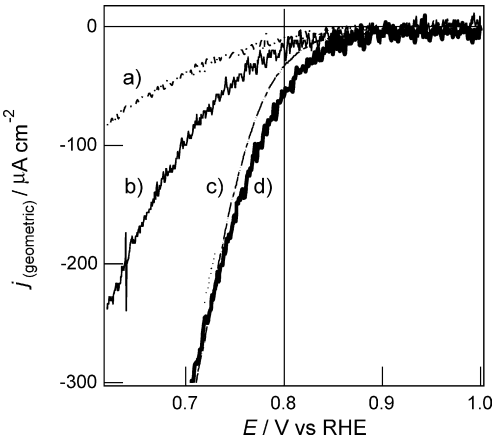

Fig. 8. ORR-current curves of the La_2O_3-treated IrO_2/Ti electrode, the IrO_2/Ti electrode and the porous $Ir_{0.6}V_{0.4}O_2$/Ti electrode. Electrodes: (a) IrO_2/Ti electrode, (b) La_2O_3-treated IrO_2/Ti electrode, (c) a platinum plate electrode, and (d) porous $Ir_{0.6}V_{0.4}O_2$/Ti electrode [31]. The preparation temperature of these oxide electrodes was 450 °C.

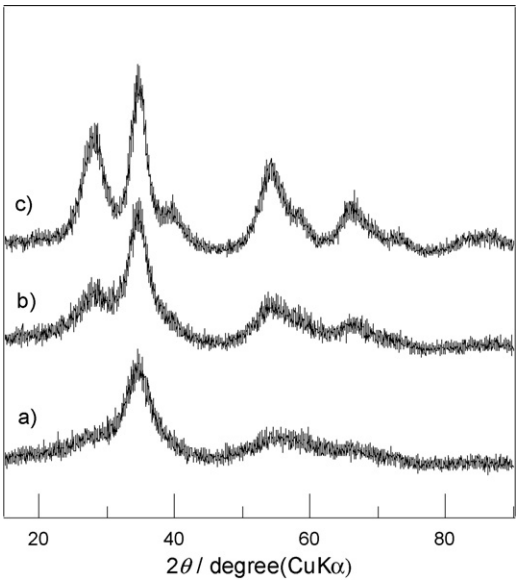

Fig. 9. XRD patterns of IrO_2 nanoparticles prepared by the Adams fusion method. Heat-treatment temperatures: (a) 400 °C, (b) 450 °C, and (c) 500 °C.

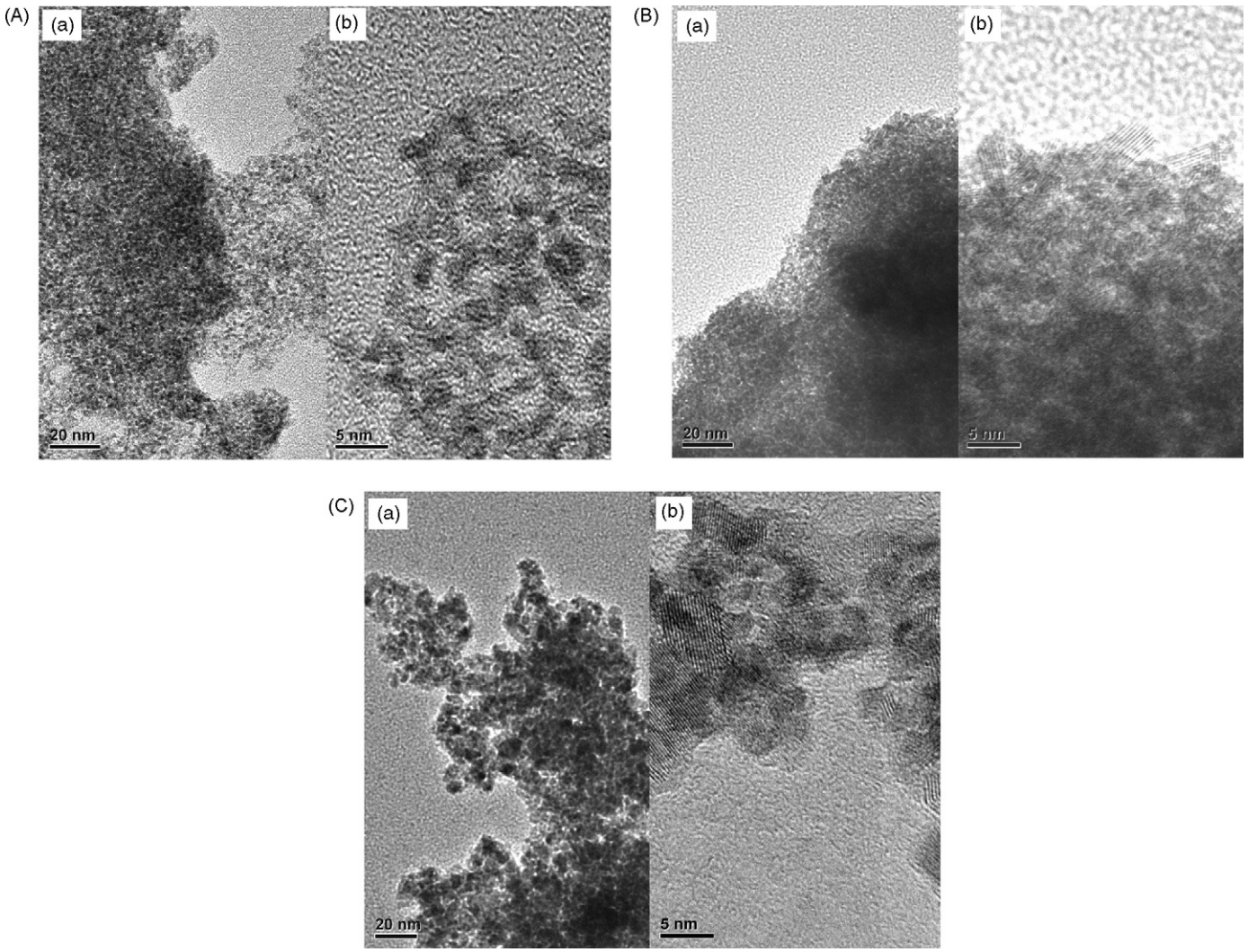

Fig. 10. (A) TEM images with different magnifications of IrO_2 nanoparticles heat-treated (A) at 400 °C, (B) at 450 °C, and (C) at 500 °C: (a) low magnification and (b): high magnification.

which was reported in the previous paper [31]. The ORR characteristics of a platinum plate electrode are also presented in Fig. 8 for comparison. The La_2O_3-treated IrO_2/Ti electrode, (b), showed higher current density for the ORR than that of the IrO_2/Ti electrode, (a), and its onset potential for the ORR, E_{ORR}, was ca. 0.88 V vs. RHE which is somewhat higher than the value of the IrO_2/Ti electrode, 0.84 V vs. RHE. As has been discussed in the previous paper [31], the porous $Ir_{0.6}V_{0.4}O_2$/Ti electrode showed the onset potentials for the ORR to be E_{ORR} = 0.90 V and $E_{ORR\text{-}20}$ = 0.86 V vs. RHE, where $E_{ORR\text{-}20}$ means the electrode potential where the oxygen reduction current attained 20 μA cm^{-2}-(geometric) [31] and exhibited twice the activity of a flat Pt plate electrode at 0.8 V (vs. RHE), when the current density for the ORR was evaluated with the geometric surface area. This oxide electrode may have a roughness factor of several decades; therefore, the actual effective surface area of this porous oxide electrocatalyst requires evaluation. Although the ORR activity of both oxide electrodes of the La_2O_3-treated IrO_2/Ti and the $Ir_{0.6}V_{0.4}O_2$/Ti were still lower than the platinum electrode, the enlargement of the surface area of the IrO_2/Ti oxide electrode with the help of lanthanum and the formation of the solid solution with appropriate other elements, vanadium in this case, can considerably enhance the catalytic activity of the IrO_2/Ti oxide electrode. When the current density for the ORR of each geometric surface area of the La_2O_3-treated IrO_2/Ti electrode shown in Fig. 7 was divided by the pseudo-capacitance, the voltammogram presented by the $j_{(ESA)}$–E curve did not rest on the group of the voltammograms shown in Fig. 5, but the voltammogram rested on about half of the $j_{(ESA)}$ for the IrO_2/Ti electrode prepared at 450 °C in the region lower than ca. 1.0 μA cm^{-2}. This deviation must be caused either by the extremely enhanced surface area or by the possibly characteristic pore structure of the IrO_2 formed by the dissolution of lanthanum oxide from the Ir–La composite oxide layer. These methods provide useful information on the design of the oxide cathode catalysts using less-expensive elements.

3.4. Characteristics of IrO_2 nanoparticles synthesized using the Adams fusion method

In order to evaluate the ORR characteristics of IrO_2 without the potential effect of titanium ions on the catalytic behavior of IrO_2/Ti electrocatalysts, iridium oxide powder was synthesized using the Adams fusion method. In Fig. 9, the XRD patterns of the IrO_2 powder heat-treated at 400 °C, 450 °C, or 500 °C for 30 min in air are presented. The intensity of the rutile-type XRD peaks increased with an increase in heat-treatment temperature; however, that of the (1 0 1) at 2θ = ca. 34.6° increased slightly, and its half-width decreased considerably with temperature, showing an increase in crystallite size. Fig. 10(A)–(C) shows the transmission electron micrographs (TEM) of these IrO_2 powders. The increase in crystallite size along with heat-treatment temperature is clearly demonstrated in these photographs. Lattice stripes are observed on the IrO_2 crystallites heat-treated at every temperature.

3.5. ORR behavior of IrO_2 nanoparticles

Fig. 11(A)–(C) shows cyclic voltammograms of the IrO_2 particles in N_2-saturated 0.5 M H_2SO_4 (broken lines) and in O_2-saturated 0.5 M H_2SO_4 (solid lines) measured in a stationary state and rotated at 2000 rpm (long- and short-dashed lines). As in the case of the IrO_2/Ti electrodes, an additional cathodic current due to the ORR was observed on each of the oxide electrodes. The apparent onset electrode potentials for the ORR (E_{ORR}) on IrO_2 heat-treated at

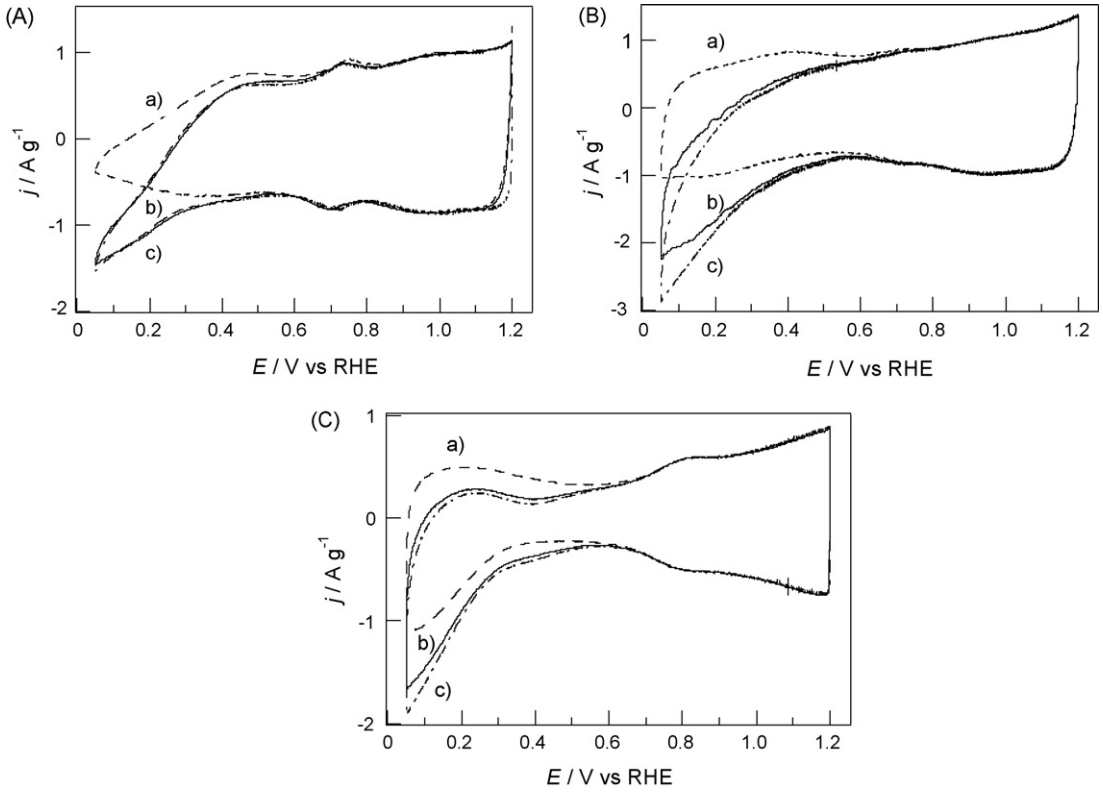

Fig. 11. (A) Cyclic voltammograms of IrO_2 nanoparticles heat-treated at 400 °C. Electrolytes: broken line (a), N_2-saturated 0.5 M H_2SO_4, 60 °C; solid line (b) and long- and short-dashed lines (c), O_2-saturated 0.5 M H_2SO_4, 60 °C. For the solid line (b), the electrode was not rotated. For the long- and short-dashed line (c), the electrode was rotated at 2000 rpm. Electrode potential sweep rate: 5 mV s^{-1}. Cyclic voltammograms of IrO_2 nanoparticles heat-treated (B) at 450 °C and (C) at 500 °C. The electrolyte, measurement conditions and nomination of the voltammograms are same as the caption of Fig. 5(a).

400 °C, 450 °C, and 500 °C were ca. 0.60 V (vs. RHE), ca. 0.69 V (vs. RHE), and ca. 0.62 V (vs. RHE), respectively. As for the reason why the onset potential for the ORR of these IrO_2 electrodes was lower than that for the IrO_2/Ti electrodes, five possible explanations could be pointed out: (1) the effects of the Nafion® ionomer; (2) the resistance between IrO_2 nanoparticles and glassy carbon, IrO_2–GC, as well as that of among IrO_2 nanoparticles contacting each other, IrO_2–IrO_2; (3) titanium ions from the oxide–Ti substrate interface; (4) the amount of the hydrated water around IrO_2 crystallites; and (5) the particle size of IrO_2. For the CV of the IrO_2/Ti electrodes, no Nafion® ionomer is needed; however, Nafion® ionomer was used for the preparation of the IrO_2 test electrodes in order to fix the IrO_2 powder to the GC surface. It has been confirmed that the addition of the Nafion® ionomer to the IrO_2 powder somewhat suppresses the catalytic activity of the catalysts for the ORR. In addition, the two possible contact resistances between IrO_2–GC and IrO_2–IrO_2 must be evaluated in future. The potential effect of the titanium ions was described above (Section 3.2). The change in the CV profiles of the IrO_2 electrodes in the N_2-saturated solution, along with heat-treatment temperature, strongly suggests that the iridium oxide nanoparticles heat-treated at 400 °C, at least, are hydrated state particles like $IrO_2 \cdot nH_2O$. Because the IrO_2 crystallites are surrounded by a water layer, the specimen must have showed lower ORR activity than the both specimens, IrO_2/Ti electrodes and IrO_2 powder electrodes heat-treated at temperatures higher than 450 °C. Ioroi et al. [44] used iridium oxide calcined at 400 °C in air as the support of platinum electrocatalyst for the unitized regenerative fuel cell (URFC), which is an electrochemical cell working both as a fuel cell and as a water electrolyzer [45]. Yao et al. also used iridium oxide as support for platinum electrocatalyst of the URFC, while Ioroi used a hydrated iridium oxide [27]. Since those iridium-supported platinum catalysts were examined as both oxygen reduction and oxygen evolution catalysts, the catalytic behavior of individual iridium oxide for the ORR has not been discussed at length in the research. The particle size of primary IrO_2 crystallites of the IrO_2/Ti electrode shown in Fig. 1(B)-(b) was 3–8 nm in diameter and those synthesized by the Adams fusion method shown in Fig. 10(A)–(C) was 3–10 nm in diameter. Therefore, it is not easy to attribute the difference of the onset potentials for the ORR between the IrO_2 particle electrodes and the IrO_2/Ti electrodes to the difference of their particle size of IrO_2. Among the five possible reasons discussed above, the forth reason, i.e. the amount of the hydrated water around IrO_2 crystallites, must be probable and predominant.

It must also be noted that only a slight deviation is observed above ca. 0.2 V (vs. RHE) between the ORR current on the electrodes rotated at 2000 rpm and on the electrodes maintained in a stationary state. That is, the comparison of the ORR current among these oxide electrodes is not meaningless, so long as we use the values in the low current density region.

Pauporté et al. investigated the valency of iridium ions in the iridium oxide film prepared by sputtering using X-ray absorption spectroscopy (XAS) at the L_3 edge of iridium atoms in 1 M H_2SO_4, and determined the valency of iridium to be between 3 and 3.85 when the potential varied from −0.2 V to + 1 V (vs. SCE) [46]. If we apply their results to our findings, the valency of the iridium ion at 0.69 V (vs. RHE) and the E_{ORR} of the IrO_2 electrode heat-treated at 400 °C correspond to about 0.35. The most important finding in this study is that IrO_2, not metallic Ir, behaves as an active catalyst for the ORR in 0.5 H_2SO_4 at 60 °C, and the highest E_{ORR} was ca. 0.84 V (vs. RHE) on the IrO_2/Ti electrodes.

4. Conclusions

The electrocatalytic ORR of iridium oxide coating prepared on a titanium substrate using a dip-coating method (IrO_2/Ti), as well as iridium oxide nanoparticles (IrO_2) prepared by the Adams fusion method, was investigated by changing the heat-treatment air temperature at the final stage of each of these methods. Although both rutile-type oxide catalysts were found to exhibit considerable activity for the ORR in 0.5 M H_2SO_4 at 60 °C, the former oxide electrodes showed greater activity than the latter ones. The most active catalyst was IrO_2/Ti heat-treated at 400 °C, showing ca. 0.84 V (vs. RHE) of the onset potential for the ORR, E_{ORR}, so long as evaluated by cyclic voltammetry. However, both the activity and the E_{ORR} seem to be almost the same among the IrO_2/Ti electrodes heat-treated at different temperatures between 400 °C and 550 °C, given the currents for the ORR on IrO_2/Ti electrodes were evaluated with their surface areas. It must be noted that IrO_2, but neither metallic Ir nor hydrated IrO_2, behaves as an active catalyst for the ORR in an acidic solution.

We have previously demonstrated that the catalytic activity of an IrO_2/Ti electrode for the ORR can be greatly enhanced by the formation of a solid solution with another element, vanadium for example, as well as with the increase in surface area [31]. The onset potential for the ORR of the $Ir_{0.6}V_{0.4}O_2$/Ti electrode was higher than that of a Pt plate electrode, although the current density was expressed with the current per geometric surface area.

The catalytic performance of rutile-type oxide of IrO_2 on the ORR may provide useful insight into how to design the oxide cathode catalyst. This investigation using iridium oxide as the cathode is the first step towards the development of less-expensive and anti-corrosive oxide cathodes in the future.

Acknowledgement

This work was supported in part by the "Polymer Electrolyte Fuel Cell Program; Development of Next Generation Technology" from the New Energy and Industrial Technology Development Organization (NEDO) of Japan.

References

[1] B.C. Beard, P.N. Ross, J. Electrochem. Soc. 137 (1990) 3368.
[2] T. Toda, H. Igarashi, H. Uchida, M. Watanabe, J. Electrochem. Soc. 146 (1999) 3750.
[3] U.A. Paulus, T.J. Schmidt, H.A. Gasteiger, R.J. Behm, J. Electrochem. Soc. 495 (2001) 134.
[4] H. Yang, W. Vogel, C. Lamy, N. Alonso-Vante, J. Phys. Chem. B 108 (2004) 11024.
[5] P. Yu, M. Pemberton, P. Plasse, J. Power Sources 144 (2005) 11.
[6] B. Wang, J. Power Sources 152 (2005) 15.
[7] J.-H. Kim, A. Ishihara, S. Mitsushima, N. Kamiya, K.-I. Ota, Electrochim. Acta 52 (2007) 2492.
[8] J. Prakash, D.A. Tryk, W. Aldred, E.B. Yeager, J. Appl. Electrochem. 29 (1999) 1463.
[9] F. Mazza, S. Trassatti, J. Electrochem. Soc. 110 (1963) 847.
[10] K. Lee, A. Ishihara, S. Mitsushima, N. Kamiya, K.-I. Ota, Electrochim. Acta 49 (2004) 3479.
[11] E. Claud, T. Addou, J.-M. Latour, P. Aldebert, J. Appl. Electrochem. 28 (1998) 57.
[12] J.P. Collman, P.S. Wagenknecht, J.E. Hutchison, Angew. Chem. Int. Ed. Engl. 33 (1994) 1537.
[13] D. Susac, A. Sode, L. Zhu, P.C. Wong, M. Teo, D. Bizzotto, K.A.R. Mitchell, R.R. Parsons, S.A. Campbell, J. Phys. Chem. B 110 (2006) 10762.
[14] K. Lee, L. Zhang, J. Zhang, Electrochem. Commun. 9 (2007) 1704.
[15] N.A. Vante, H. Tributsch, Nature 323 (1986) 431.
[16] O. Savadogo, K. Lee, K. Oishi, S. Mitsushima, N. Kamiya, K.-I. Ota, Electrochem. Commun. 6 (2004) 105.
[17] A. Ishihara, K. Lee, S. Doi, S. Mitsushima, N. Kamiya, M. Hara, K. Domen, K. Fukuda, K.-I. Ota, Electrochem. Solid-State Lett. 8 (2005) A201.
[18] Y. Liu, A. Ishihara, S. Mitsushima, N. Kamiya, K.-I. Ota, Electrochem. Solid-State Lett. 8 (2005) A400.
[19] J. Rolewicz, Ch. Comminellis, E. Plattner, J. Hinden, Chimia 42 (1988) 75.
[20] J. Rolewicz, Ch. Comminellis, E. Plattner, J. Hinden, Electrochim. Acta 33 (1988) 573.
[21] K. Kameyama, K. Tsukada, K. Yahikozawa, Y. Takasu, J. Electrochem. Soc. 141 (1994) 643.
[22] D.S. Gnanamuthu, J.V. Petrocelli, J. Electrochem. Soc. 114 (1967) 1036.
[23] A.J. Appleby, J. Electroanal. Chem. 27 (1970) 325.
[24] K. Lee, L. Zhang, J. Zhang, J. Power Sources 165 (2007) 108.

[25] K. Lee, L. Zhang, J. Zhang, J. Power Sources 170 (2007) 291.
[26] T. Ioroi, K. Kitazawa, K. Yasuda, Y. Yamamoto, H. Takenaka, J. Electrochem. Soc. 147 (2000) 2018.
[27] W. Yao, J. Yang, J. Wang, Y. Nuli, Electrochem. Commun. 9 (2007) 1029.
[28] C.-C. Chang, T.-C. Wen, J. Electrochem. Soc. 143 (1996) 1485.
[29] C.-C. Chang, T.-C. Wen, Mater. Chem. Phys. 47 (1997) 203.
[30] Y. Takasu, W. Sugimoto, M. Yoshitake, Electrochemistry 75 (2007) 105.
[31] Y. Takasu, N. Yoshinaga, W. Sugimoto, Electrochem. Commun. 10 (2008) 668.
[32] Y. Murakami, T. Kondo, Y. Shimoda, H. Kaji, K. Yahikozawa, Y. Takasu, J. Alloys Compd. 239 (1996) 111.
[33] Y. Murakami, T. Nakamura, X.-G. Zhang, Y. Takasu, J. Alloys Compd. 259 (1997) 196.
[34] R. Adams, R. Shriner, J. Am. Chem. Soc. 45 (1923) 2171.
[35] T.J. Schmidt, U.A. Paulus, H.A. Gasteiger, R.J. Behm, J. Electroanal. Chem. 508 (2001) 41.
[36] U.A. Paulus, T.J. Schmidt, H.A. Gasteiger, R.J. Behm, J. Electroanal. Chem. 495 (2001) 134.
[37] B.E. Conway, J. Electrochem. Soc. 138 (1991) 1539.
[38] S. Trasatti, P. Kurzweil, Platinum Met. Rev. 38 (1994) 46.
[39] T. Arikawa, Y. Takasu, Y. Murakami, K. Asakura, Y. Iwasawa, J. Phys. Chem. B 102 (1998) 3736.
[40] K. Tsukada, K. Kameyama, K. Yahikozawa, Y. Takasu, Kagaku Denki (presently Electrochemistry) 61 (1993) 435.
[41] L.D. Burke, E.J.M. O'Sullican, J. Electroanal. Chem. 117 (1989) 155.
[42] P. Siviglia, A. Daghetti, S. Trasatti, Colloids Surf. 7 (1983) 15.
[43] S. Lavine, A.L. Smith, Discuss. Faraday Soc. 128 (1981) 2141.
[44] T. Ioroi, K. Kitazawa, K. Yasuda, Y. Yamamoto, H. Takenaka, J. Appl. Electrochem. 31 (2001) 1179.
[45] F. Mitlitsky, B. Myers, A. Weisberg, Energy Fuels 12 (1998) 56.
[46] T. Pauporté, D. Aberdam, J.-L. Hazemann, R. Faure, R. Durand, J. Electroanal. Chem. 465 (1999) 88.